ELSEVIER

Physics of the Earth and Planetary Interiors 99 (1997) 55–67

PHYSICS OF THE EARTH AND PLANETARY INTERIORS

Thermal convection in rotating spherical shells

M. Ardes *, F.H. Busse, J. Wicht

Institute of Physics, University of Bayreuth, D-95440 Bayreuth, Germany

Received 26 February 1996; accepted 15 May 1996

Abstract

Linear and non-linear properties of thermal convection in rotating spherical shells of varying radius ratios are investigated numerically. The range of validity of the simple 'equatorial' approximation is determined through a comparison with the more complete numerical analysis based on the Galerkin approximation. The earlier work of Zhang and Busse (1987, *Geophys. Astrophys. Fluid Dyn.*, 39: 119–147) is extended in order to classify the way in which different modes of convection become preferred in various parts of the parameter space. It is found that in the transition region between equator attached convection and columnar convection an intermediate mode with a multi-humped structure enters. Examples of non-linear vacillating convection in low Prandtl number fluids are discussed.

1. Introduction

Because of its importance for the transport of energy in the interiors of stars and planets the problem of thermal convection in rotating spherical shells has become one of the fundamental fluid dynamical problems in geophysics and astrophysics. In spite of the considerable literature on the problem going back for several decades (see, for instance, Chandrasekhar, 1961), the problem has still not been fully understood and many open questions remain. The main mathematical difficulties arise from the fact that the preferred mode is usually non-axisymmetric and time dependent even at the onset of convection. In addition the relatively large number of parameters that are necessary to describe even the most simple version of the problem have complicated its investigation.

Early work on the linear problem of the onset of convection in rotating spheres and spherical shells was restricted to axisymmetric solutions (Chandrasekhar, 1961, and references therein). It later became obvious that axisymmetric convection is preferred only in a very small region of the parameter space (Roberts, 1968; Geiger and Busse, 1981) and that the preferred azimuthal wavenumber grows strongly with increasing rate of rotation. The asymptotic analysis of the non-axisymmetric problem for high rates of rotation was introduced by Roberts (Roberts, 1965, Roberts, 1968) and the preferred mode of convection was identified by Busse (1970a). Because convection and other flows in rapidly rotating systems are dominated by the Proudman–Taylor theorem, the preferred mode of convection assumes a relatively simple two-dimensional structure at high rates of rotation. Nevertheless, it is difficult to capture this structure in a numerical analysis because the typical length scales in the directions perpendicular to the axis of rotation decrease strongly with increasing

* Corresponding author.

PII S0031-9201(96)03200-1

Taylor number. For this reason many attempts have been made to obtain analytical approximations in special cases. In the case of a thin shell the effects of rotation can be treated as a perturbation (Busse, 1970b, Busse, 1973) without restricting the validity of the results to small rotation rates only. In a sense the 'equatorial' approximation used in the present paper can be regarded as an extension of that earlier perturbation analysis. Another analytical method for the description of low Prandtl number convection in rotating spheres is based on the property that thermal convection in a rotating system can be considered as a perturbation of inertial oscillations (Zhang, 1994). The results obtained with the equatorial approximation also show similarities with some of the preferred inertial modes.

While the equatorial approximation reduces the linear problem of the onset of convection to the integration of ordinary differential equations in the radial coordinate, the full solution of the linear problem requires the solution of partial differential equations depending on two coordinates. A Galerkin scheme has often been used for this purpose and the most detailed calculations have been done by Zhang and Busse (1987). Some of the findings of the latter paper are the starting points of the numerical analysis described in the present paper. The competition between the equatorially attached modes and the spiralling mode of convection is investigated in more detail and all results are extended to higher values of the Taylor number.

The paper starts with a short description of the mathematical problem and introduces the main methods of the analysis in Section 2. The equatorial approximation is discussed in Section 3 and its results are compared in Section 4 with the results based on the Galerkin approximation. An overview of the various modes at high Taylor numbers is given in Section 5 and some results obtained for finite amplitude convection are presented in Section 6. The paper closes with a concluding discussion in Section 7.

2. Mathematical formulation of the problem

Following earlier analyses we consider the problem of convection in rotating spherical shells in its classical formulation with a uniform distribution of heat sources and a gravity force that increases with distance from the center of the sphere. Accordingly the distributions of temperature and gravity in the spherically symmetric basic state are given by

$$T = T_0 - \beta \tilde{r}^2/2, \quad \boldsymbol{g} = -\gamma \tilde{\boldsymbol{r}} \tag{1}$$

where $\tilde{\boldsymbol{r}}$ is the position vector with respect to the center of the sphere and $\tilde{r}$ is its absolute value. The sphere is rotating with angular velocity Ω about a fixed axis given by the unit vector $\boldsymbol{k}$. It will be convenient to introduce dimensionless variables. As length scale we use the difference d between inner and outer radius of the spherical fluid shell. As time scale we use d^2/ν where ν is the kinematic viscosity of the fluid and as temperature scale we take $\beta d^2 \nu/\kappa$ where κ denotes the thermal diffusivity of the fluid. The dimensionless equations of motion for the velocity vector $\boldsymbol{u}$ and the heat equation for the deviation Θ of the temperature from the static distribution are given by

$$\frac{\partial}{\partial t}\boldsymbol{u} + \boldsymbol{u}\cdot\nabla\boldsymbol{u} + \tau\boldsymbol{k}\times\boldsymbol{u} = -\nabla\pi + rR\Theta + \nabla^2\boldsymbol{u} \tag{2a}$$

$$\nabla\cdot\boldsymbol{u} = 0 \tag{2b}$$

$$\left(\frac{\partial}{\partial t}\Theta + \boldsymbol{u}\cdot\nabla\Theta\right)P = \boldsymbol{r}\cdot\boldsymbol{u} + \nabla^2\Theta \tag{2c}$$

where $\boldsymbol{r}$ is the dimensionless position vector and the Rayleigh number R, the Taylor number τ^2, and the Prandtl number P are defined by

$$R = \frac{\alpha\gamma\beta d^6}{\nu\kappa}, \quad \tau = \frac{2\Omega d^2}{\nu}, \quad P = \frac{\nu}{\kappa}$$

The thermal expansivity has been denoted by α and the Boussinesq approximation has been assumed. In order to eliminate the continuity Eq. (2a) we introduce the general representation for the solenoidal vector field $\boldsymbol{u}$,

$$\boldsymbol{u} = \nabla\times(\nabla\times r v) + \nabla\times r w \tag{3}$$

where the scalar variables v, w are uniquely defined if the condition is imposed that their averages over surfaces r = const. vanish. By multiplying the curl-

curl and the curl of Eq. (2a) with $\boldsymbol{r}$ we obtain two equations for v and w,

$$\left[\left(\nabla^2-\frac{\partial}{\partial t}\right)L_2+\tau\boldsymbol{k}\times\boldsymbol{r}\cdot\nabla\right]\nabla^2 v+\tau Q w - RL_2\Theta=-\boldsymbol{r}\cdot\nabla\times(\nabla\times(\boldsymbol{u}\cdot\nabla\boldsymbol{u})) \quad (4a)$$

$$\left[\left(\nabla^2-\frac{\partial}{\partial t}\right)L_2+\tau\boldsymbol{k}\times\boldsymbol{r}\cdot\nabla\right]w-\tau Q v =\boldsymbol{r}\cdot\nabla\times(\boldsymbol{u}\cdot\nabla\boldsymbol{u}) \quad (4b)$$

where L_2 is the negative Laplacian on the unit sphere and Q is defined by

$$Q\equiv\boldsymbol{k}\cdot\nabla-\frac{1}{2}(L_2\boldsymbol{k}\cdot\nabla+\boldsymbol{k}\cdot\nabla L_2) \quad (5)$$

We shall assume stress-free isothermal conditions at the spherical boundaries,

$$v=\frac{\partial^2}{\partial r^2}v=\frac{\partial}{\partial r}\left(\frac{w}{r}\right)=\Theta=0 \text{ at } r=r_i\equiv\frac{\eta}{1-\eta} \text{ and } r=r_0\equiv\frac{1}{1-\eta} \quad (6)$$

where η denotes the radius ratio of the spherical shell.

In order to solve Eq. (4a), Eq. (4b) and Eq. (2c) it is convenient to introduce spherical coordinates r, θ, φ and expand the dependent variables into complete systems of functions satisfying the boundary conditions Eq. (6),

$$v=\sum_{\nu,l,n}a_{\nu nl}\exp\{i(\nu m\varphi+\omega t)\}P_l^{|\nu|m}(\cos\theta)\times\sin n\pi(r-r_i) \quad (7a)$$

$$w=r\sum_{\nu,\hat{l},n}c_{\nu n\hat{l}}\exp\{i(\nu m\varphi+\omega t)\}P_{\hat{l}}^{|\nu|m}(\cos\theta)\times\cos(n-1)\pi(r-r_i) \quad (7b)$$

$$\Theta=\sum_{\nu,l,n}b_{\nu nl}\exp\{i(\nu m\varphi+\omega t)\}P_l^{|\nu|m}(\cos\theta)\times\sin n\pi(r-r_i) \quad (7c)$$

This representation has been chosen in such a way that solutions in the form of drifting waves which are m-periodic in the azimuthal direction are described by constant coefficients $a_{\nu ln}$ etc. More complex solutions can be described by time dependent coefficients $a_{\nu ln}$ etc. In both cases the conditions

$$a_{\nu\ln}=a^+_{-\nu\ln},\quad b_{\nu\ln}=b^+_{-\nu\ln},\quad c_{\nu\hat{l}n}=c^+_{-\nu\hat{l}n} \quad (8)$$

must be satisfied for real expressions Eqs. (7a), (7b) and (7c) where the superscript + indicates the complex conjugate. Of particular interest are solutions that are symmetric with respect to the equatorial plane in which case the subscript l runs through $|\nu|m+2j$ for $j=0, 1, 2 \ldots$ while the subscript $\hat{l}$ runs through $|\nu|m+2j+1$ for the same j. The associated Legendre polynomials will be assumed in such a form that the average of $[P_l^\mu]^2$ over the unit sphere is unity.

After the equations for the coefficients $a_{\nu ln}$ etc. have been obtained through a projection of the basic equations Eq. (4a), Eq. (4b) and Eq. (2c) onto the space of the expansion functions used in Eqs. (7a), (7b) and (7c) the system of equations for the coefficients must be truncated. We shall use the truncation condition that all coefficients and corresponding equations are neglected whose subscripts satisfy

$$2n+l-|\nu|m+2|\nu|>3+2N_T \quad (9)$$

The same condition applies for $\hat{l}$ instead of l. The condition is the same as used by Zhang and Busse (1987) and provides a triangular truncation such that as many functions in the radial as in the latitudinal direction are used for the representation of the solution.

For the linear problem of the onset of convection the right hand side of Eq. (4a) and Eq. (4b) and the term $\boldsymbol{u}\cdot\nabla\Theta$ in Eq. (2c) can be neglected and only terms with $\nu=1$ need to be kept in the representation Eqs. (7a), (7b) and (7c). The linear homogeneous system of complex algebraic equations for the coefficients a_{1ln} represents an eigenvalue problem for R and ω as the real and imaginary parts of the eigenvalue.

3. The equatorial approximation

In many situations it can be observed that the preferred solutions of the linear problem are described by

$$v=\exp\{im\varphi+i\omega t\}P_m^m(\cos\theta)f(r)+\ldots \quad (10a)$$

$$w = \exp\{im\varphi + i\omega t\} P^m_{m+1}(\cos\theta)\, g(r) + \ldots \quad (10b)$$

$$\Theta = \exp\{im\varphi + i\omega t\} P^m_m(\cos\theta)\, h(r) + \ldots \quad (10c)$$

where the explicitly denoted leading terms are much larger than the following ones. In the case of low rotation rates solutions of the form Eqs. (10a), (10b) and (10c) are obtained for the preferred convection mode when a perturbation expansion in the parameter τ is used (Busse, 1973). The dispersion relation

$$\omega = \frac{\tau}{(m+1)(1+P)} \quad (11a)$$

holds and the expression

$$R = \frac{(\pi^2+\alpha^2)^3}{\alpha^2} + \tau^2 \frac{\pi^2+\alpha^2}{(2m+3)\alpha^2} \times \left(1 + \frac{4\pi^2/\alpha}{\pi^2+\alpha^2}\coth\frac{\alpha}{2}\right) + \ldots \quad (11b)$$

is obtained in the small gap limit $r_i \to \infty$ with $\alpha \equiv m/r_i$. As in ordinary Rayleigh–Bénard convection the critical wavenumber α corresponds to $\alpha_c = \pi\sqrt{2}$. Here we enter with the ansatz Eqs. (10a), (10b) and (10c) directly into Eq. (4a), Eq. (4b) and Eq. (2c) and obtain

$$\left[\left(\frac{1}{r}\left(\frac{d^2}{dr^2}r - \frac{L_2}{r}\right) - i\omega\right) L_2 + im\tau\right]\frac{1}{r} \times \left(\frac{d^2}{dr^2}r - \frac{L_2}{r}\right) f - \tau\frac{m(m+2)(2m+1)}{2m+3} \times \left(\frac{d}{dr}g + \frac{m+2}{r}g\right) - RL_2 h = 0 \quad (12a)$$

$$\left[\left(\frac{1}{r}\left(\frac{d^2}{dr^2}r - \frac{L_2^*}{r}\right) - i\omega\right) L_2^* + im\tau\right] g + \tau\frac{m(m+2)}{2m+1}\left(\frac{d}{dr}f - \frac{m}{r}f\right) = 0 \quad (12b)$$

$$\left(\frac{1}{r}\left(\frac{d^2}{dr^2}r - \frac{L^2}{r}\right) - i\omega P\right) h + L_2 f = 0 \quad (12c)$$

The abbreviations $L_2 = m(m+1)$, $L_2^* = (m+1)(m+2)$ have been used in writing these expressions. The only approximation that has been made in the derivations of these equations is the neglection of the term proportional to P^m_{m+2} which appears in the evaluation of Qw. But since this term is of the order m^{-1} smaller than the term that has been retained, the approximation should become exact in the limit of high wavenumbers m. The main advantage of the reduced problem Eqs. (12a), (12b) and (12c) is that ordinary differential equations have to be solved subject to the boundary conditions

$$f = f'' = \left(\frac{g}{r}\right)' = h = 0 \quad \text{at} \quad r = r_i, r_0 \quad (13)$$

instead of the partial equations of the original formulation. The simple functional dependence of the mode Eqs. (10a), (10b) and (10c) allows also a more direct interpretation of the physical properties of this type of convection than is possible on the basis of the more complex Galerkin representation Eqs. (7a), (7b) and (7c). In the following we shall solve Eqs. (12a), (12b) and (12c) together with the boundary conditions Eq. (13) with a Runge–Kutta shooting method (Press et al., 1986) and compare the results with the more complete analysis of the linear version of the problem Eq. (4a), Eq. (4b) and Eq. (2c) based on the Galerkin scheme.

It is of interest to evaluate Eqs. (12a), (12b) and (12c) in the limit of vanishing dissipation in which case solutions can be obtained for $R = 0$. The elimination of g yields in this case the following equation for f,

$$\left\{(\omega L_2^* - \tau m)(\omega L_2 - \tau m) - \tau^2\frac{m^2(m+2)^2}{2m+3}\right\}\left(\frac{d^2}{dr^2}r - \frac{L_2}{r}\right) f = 0 \quad (14)$$

It is of interest to note that the r-dependence is independent of the rotation rate and of the frequency ω of oscillation in this case. Since the Laplace operator acting on v must not vanish because of the boundary conditions, Eq. (14) demands that the wavy

bracket equals zero. From this condition we obtain the dispersion relation

$$\frac{\omega}{\tau} = \frac{1}{m+2}\left(1 \pm \left[1 + m(m+2)(2m+3)^{-1}\right]^{\frac{1}{2}}\right) \tag{15}$$

Remarkably, this dispersion relation does not depend on the radius ratio of the spherical shell. The relationship Eq. (15) agrees for all m with the dispersion relation for equatorially symmetric inertial waves as can be seen, for example, by a comparison with expressions (4.1) and (4.5) of Zhang (1994). The neglection of the term proportional to P^m_{m+2} is thus not important in the limit of small Prandtl numbers where the convection modes approach closely the form of inertial waves for large values of τ.

4. Comparison of the equatorial approximation and Galerkin results

In this section we compare the results obtained on the basis of Eqs. (10a), (10b) and (10c) and Eqs. (12a), (12b) and (12c) with those resulting from the Galerkin approach based on the representation Eqs. (7a), (7b) and (7c). We expect that the equatorial approximation works well for relative small Taylor numbers τ^2 and will be especially useful in the case of the equatorial modes which are preferred at low Prandtl number. In Fig. 1 results for $P = 10$ are shown which demonstrate that the equatorial approximation works well up to Taylor numbers τ^2 of the order 10^5. The asymptotic relationships for high Taylor numbers differ since the formation of convection columns can not be described by the equatorial approximation.

In Fig. 2 results for $P = 0.1$ are plotted in the case $m = 10$. The curves clearly show the mode switching phenomenon demonstrated by Zhang and Busse (1987) for the mode of lowest Rayleigh number for a given m. The mode corresponding to a prograde drift (negative ω) is preferred at high τ. Only at very low values of P the mode with retrograde drift will become preferred as pointed out by Zhang (1994). The frequencies approach rather closely the inertial frequencies given by Eq. (15). As expected this approach becomes much closer as the Prandtl number is decreased. The third mode which approximately retains the frequency of the low τ limit does not correspond to an inertial oscillation. This property is also apparent from the strong increase of the

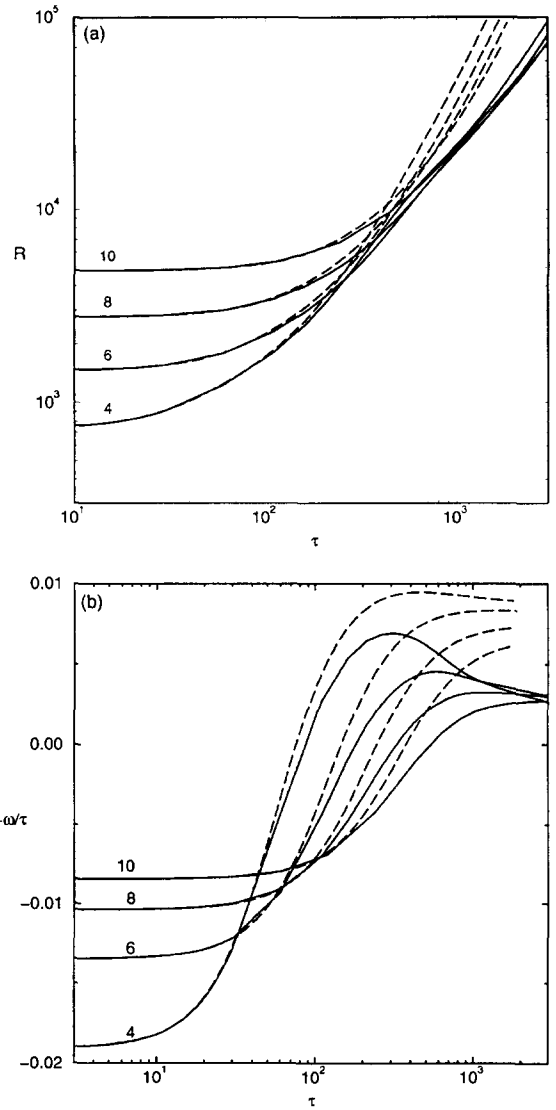

Fig. 1. (a) The Raleigh number R as a function of τ in the case $P = 10, \eta = 0.4$ for different values of m as indicated on the curves. Results based on the equatorial approximation (dashed curves) are shown in comparison with the results obtained with the Galerkin scheme (solid lines). (b) The frequency ω is shown for the same solutions as in Fig. 1a.

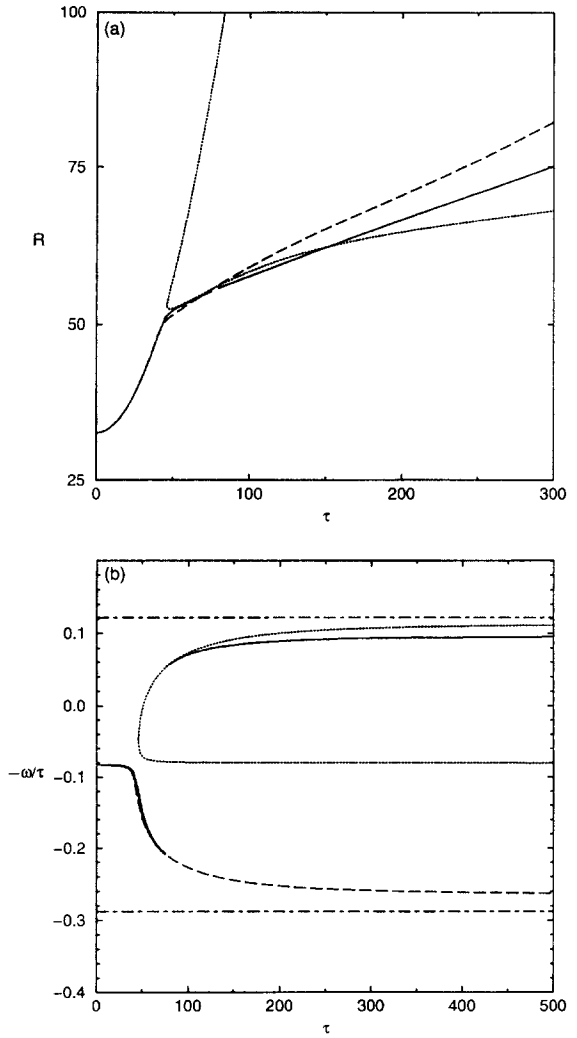

Fig. 2. (a) The Raleigh number R as a function of τ in the case $P = 0.1, \eta = 0.8, m = 10$. The results of the Galerkin computations (solid line) are shown only for the solution with the lowest value of R. The results obtained on the basis of the equatorial approximation (dashed and dotted curves) indicate that there are two different eigenmodes whose Rayleigh number curves intersect. (b) The frequency ω corresponding to the curves shown in Fig. 2a. In addition the asymptotic values given by Eq. (15) are shown (dash-dotted lines).

Rayleigh number shown in Fig. 2(a). Similar graphs have been obtained for other values of the radius ratio η, but are not displayed here since the quality of the equatorial approximation does not seem to depend much on the parameter η. Only as η approaches unity, the approximation remains valid to significantly higher values of τ.

5. Onset of convection at high Taylor numbers

The results to be discussed in this and the following sections are based on the Galerkin method. Through the use of a sufficiently high truncation parameter N_T, a range of high Taylor numbers can be reached where asymptotic relationships become valid. In Fig. 3 an overview of the numerical results is given in the case $\eta = 0.4$. The critical value R_c of the Rayleigh number is plotted in Fig. 3(a), the corresponding frequencies ω_c and corresponding azimuthal wavenumbers m_c are shown in Fig. 3(b) and (c). Since the asymptotic scaling is used, all these quantities tend to approach constant values in the average for high τ. But in their details the figures exhibit considerable structure especially in the low Prandtl number cases. Contrary to expectation the preferred wavenumber m does not always increase monotonically with τ and the frequency also exhibits some jumps for low Prandtl numbers which indicate a change in the style of convection.

In Fig. 4 the situation in the neighborhood of one of the regions of non-monotonic dependence is shown in detail. The kinks in the curves for different values of m in Fig. 4(a) correspond to transitions in the eigenvectors. This property is especially evident in the discontinuities of the corresponding frequencies as shown in Fig. 4(b). According to the streamlines displayed in Fig. 4(c), the equatorially attached convection mode realized for low values of τ become first displaced by a double-humped mode at $\tau = 5000$ which itself is superseded by the columnar convection mode at about $\tau = 11\,500$. The intermediate mode exhibits its double-humped nature also at the surface of the sphere as shown in Fig. 4(d). The streamlines at the surface reflect the geometry of the streamlines in the equatorial plane because of the approximately two-dimensional character of the solution induced by the Taylor–Proudman condition. The transition regime of an intermediate mode between the equatorially attached mode and the columnar mode persists as the analysis is extended to lower Prandtl numbers. Our findings are displayed in Fig. 5 which represents a refinement and extension

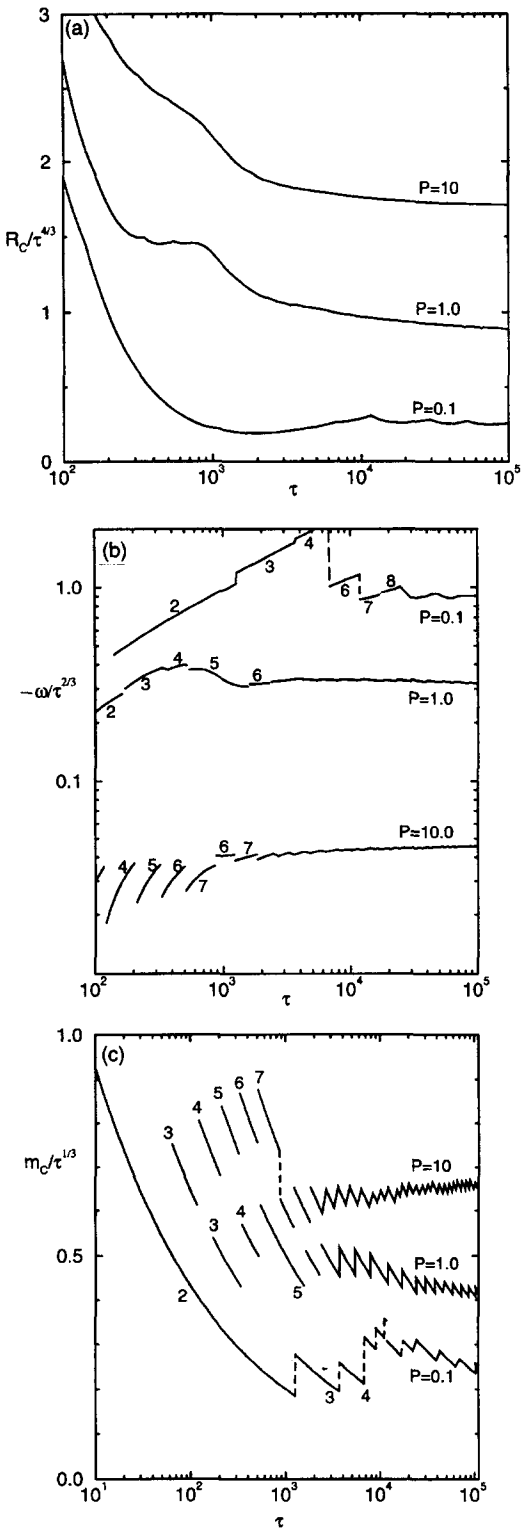

of a corresponding figure in the paper of Zhang and Busse (1987). According to Fig. 5 the Taylor number τ^2 of the transition region increases in proportion to $P^{-1/4}$ for small P. The changes in the structure of the convection modes with increasing Taylor number become even more pronounced as the Prandtl number is decreased. A typical example for $P = 10^{-2}$ is shown in Fig. 6. The changes from the equator-attached mode to the multi-hump structure at intermediate Taylor numbers and finally to the spiralling columns attached to the cylindrical surface touching the inner sphere at the equator are quite dramatic. The small scale structure seen in the plots could be interpreted as a sign of insufficient numerical resolution. But special care was taken through the use of quadruple precision, and the truncation parameter has been increased up to $N_T = 30$ in order to obtain an approximation that does not change noticeably if the truncation is increased even further. According to Eq. (9) $N_T = 30$ corresponds to a total of 2970 coefficients.

6. Convection at finite amplitudes

The properties of convection at the onset as determined by linear theory are also exhibited by finite amplitude solutions obtained for Rayleigh numbers beyond the critical value. In the parameter regime that has been investigated, only supercritical bifurcations were found even at low Prandtl numbers for which the bifurcation in a horizontal layer heated from below and rotating about a vertical axis is usually subcritical (Veronis, 1968; Clever and Busse, 1979). A number of new features enter, however, as the evolution of convection flows is pursued to higher Rayleigh numbers. The features are caused by the non-linear interaction of different modes as shown, for example, in Fig. 7. Onset in the form of a

Fig. 3. (a) The critical value R_c of the Rayleigh number as a function of τ in the case $\eta = 0.4$ for three different values of the Prandtl number as indicated. (b) The frequency ω corresponding to the curves of Fig. 3a. The integer numbers denote the corresponding value of m_c. (c) The critical wavenumber m_c corresponding to the curves of Fig. 3a.

mode with $m = 3$ is preferred in this case. But the critical value R_2 of the Rayleigh number for the mode with $m = 2$ is only little higher and the latter replaces the $m = 3$ mode as soon as the Rayleigh number exceeds R_2 slightly. Since the $m = 2$ mode is stable for $R > R_2$ there is a finite region where both, the $m = 2$ and the $m = 3$ modes can be realized depending on the initial conditions. The $m = 2$ modes becomes unstable owing to an oscillatory instability which leads to vacillating convection. The oscillation can be understood as onset of an $m = 1$ component of convection which propagates relative to the $m = 2$

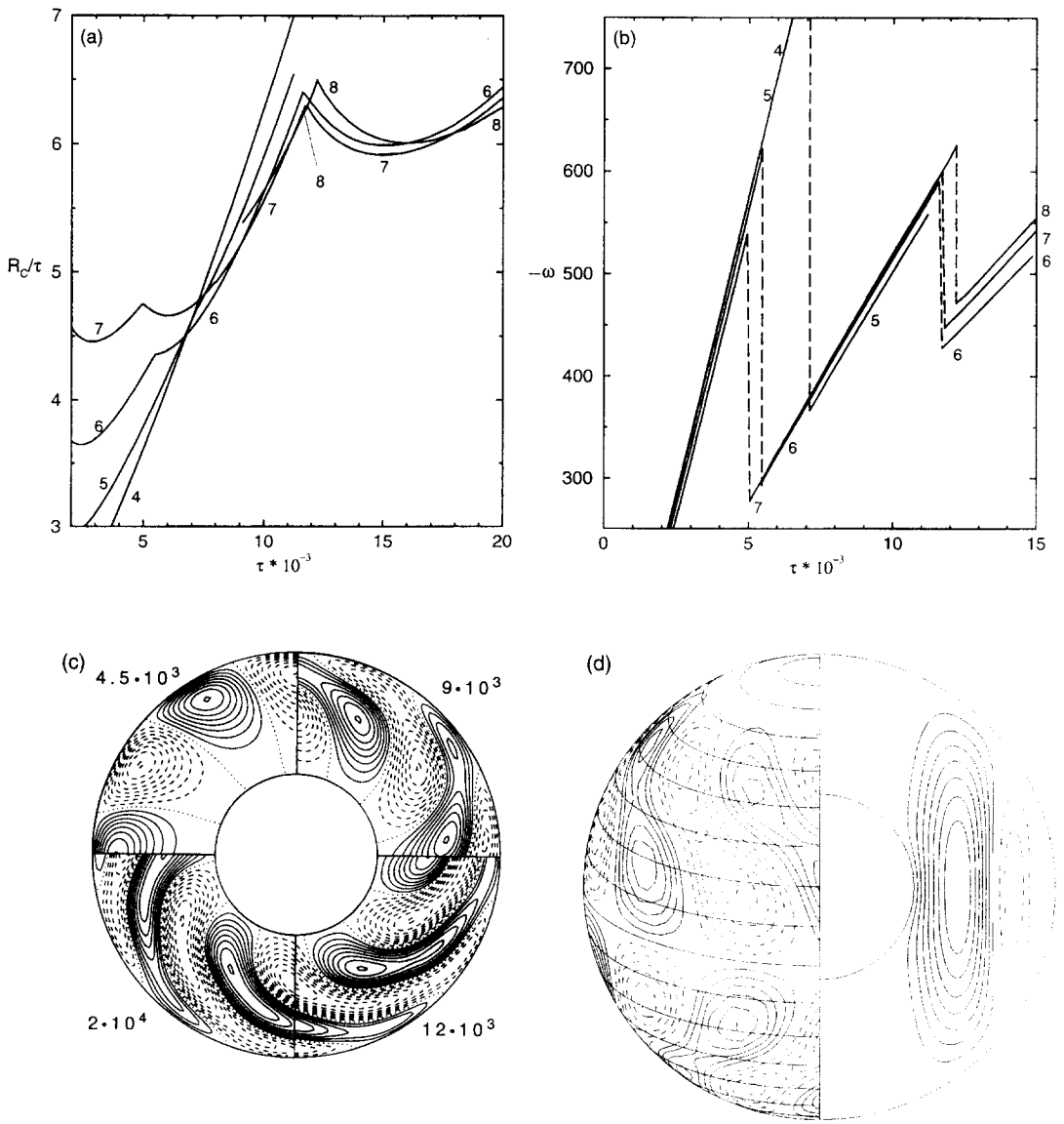

Fig. 4. (a) The Rayleigh numbers for the onset of different modes of convection corresponding to different values of m as indicated in the case $P = 0.1, \eta = 0.4$. (b) The frequencies ω corresponding to the curves of Fig. 4a. (c) The streamfunction $r\delta v/\delta\varphi$ in the equatorial plane for the different branches of eigenfunctions with $m = 6$ in Fig. 4a with values of τ as indicated. (d) Streamlines w = const. at the surface of the spherical shell (left half) and lines of constant temperature deviation Θ in the plane $\varphi = 0$ (right half) for $\tau = 9 \times 10^3$, R = 47696.1, P = 0.1. The driftrate is $c = 77.79$ in this case.

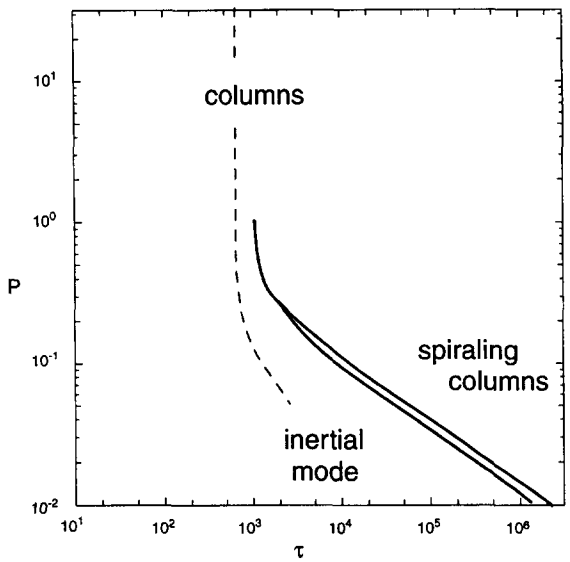

Fig. 5. Regimes of different types of convection at onset in the P-τ-plane. The dashed line indicates roughly the upper value of τ up to which the equatorial approximation holds.

mode in the prograde direction as shown in Fig. 8. Because the plots of the figure have been drawn for the reference system which is fixed to the drifting $m = 2$ mode, the much weaker $m = 1$ component with its higher drift rate moves in the counter-clockwise direction. At some higher Rayleigh number when the critical Rayleigh number for the $m = 1$ mode has been exceeded, the convection returns to a

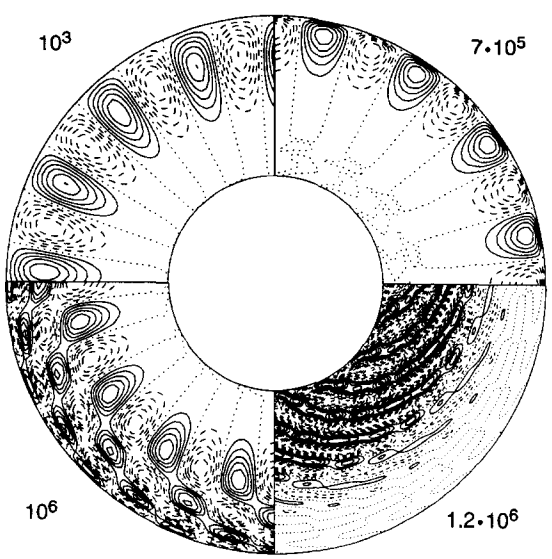

Fig. 6. The streamfunction $r\delta v/\delta\varphi$ in the equatorial plane for the mode with $m = 16$ at different rotation rates in the case $P = 0.01$ for the values of τ as indicated. Truncation parameters up to $N_T = 30$ have been used.

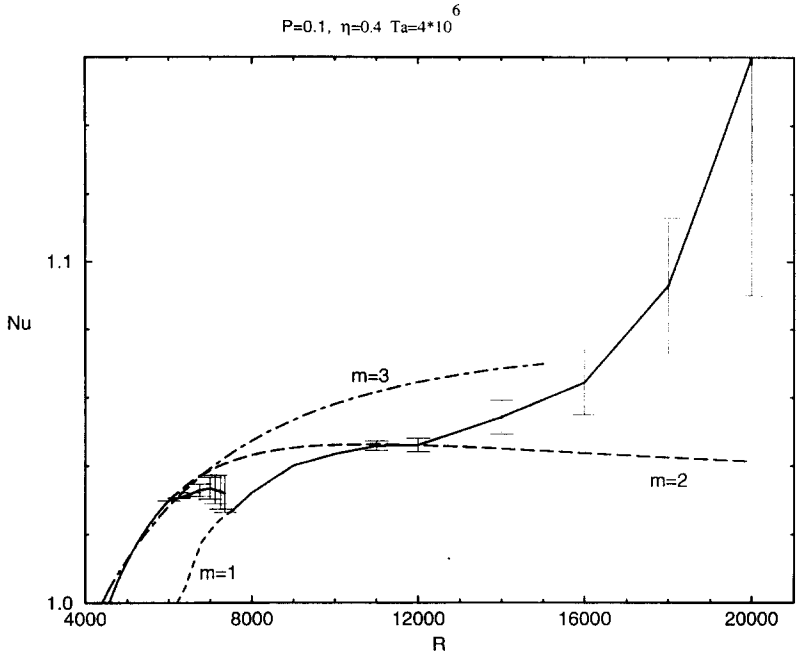

Fig. 7. Nusselt number Nu as a function of the Rayleigh number R for different modes of convection in the case $\tau = 2000, P = 0.1, \eta = 0.4$. The modes correspond to different wavenumbers m as indicated and their Nusselt number is shown by a solid line where they are stable. Dashed lines are used where they are unstable. Straight lines have been used at higher Rayleigh numbers where computations have been carried out only at discrete points. In the case of vacillations the bars indicate maximum and minimum values of the Nusselt number during an oscillation.

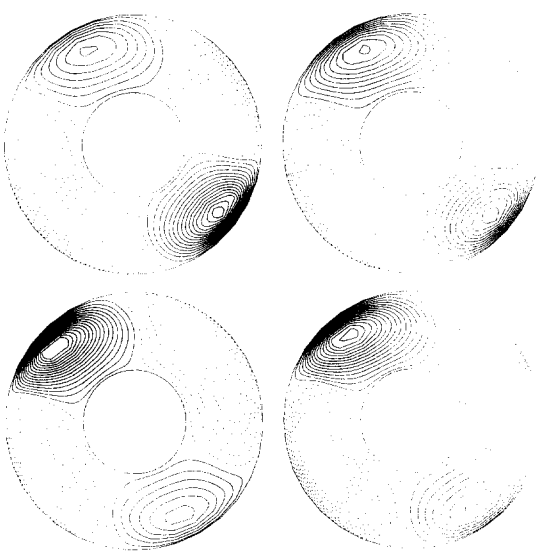

Fig. 8. The streamlines corresponding to constant values of $r\delta v/\delta\varphi$ in the equatorial plane at the times 0,0.0023,0.0046,0.0069 (clockwise from upper left) such that a half period of length 0.081 is covered if the first plot is turned by 180°. The half period of the convection velocity corresponds to a full period of the Nusselt number. The parameters are $R = 7350, \tau = 2 \times 10^3, P = 0.1$. The drift rate is $c = 104$.

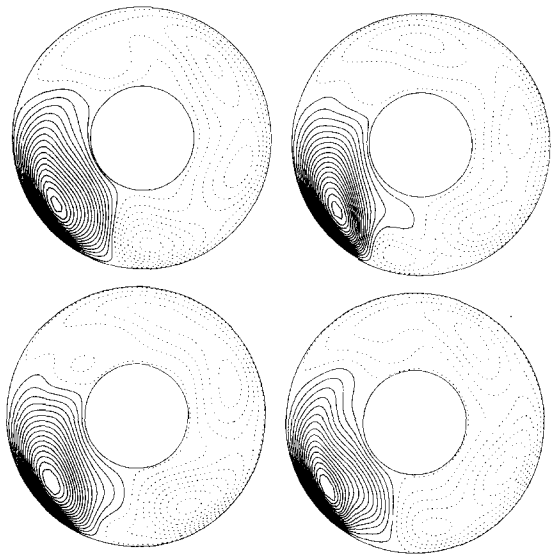

Fig. 9. Same as Fig. 8, but for $R = 1.4 \times 10^4$. The times of the four plots are $0, 4.4 \times 10^{-3}, 8.9 \times 10^{-3}, 13.2 \times 10^{-3}$ (clockwise from upper left). The drift rate is $c = 159$.

stationarily drifting form of flow with a pure $m = 1$ pattern. With a further increase of the Rayleigh number a bifurcation to a vacillating form of convection occurs again and the stationary $m = 1$ mode becomes unstable. In Fig. 9 a period of these vacillation is visualized indicating a strong cyclonic vortex. On the retrograde side of this vortex weaker vortices of opposite sign emerge into the broad anticyclonic region, travel in the retrograde direction until they disappear on the prograde side of the cyclone. While initially the onset of oscillations tends to decrease the heat transport, it can be noticed from Fig. 7 that the vacillations soon lead to an increase of the heat transport in comparison to that of the stationary $m = 1$ mode. The convection remains periodic in time up to Rayleigh numbers of the order of $1.5 \cdot 10^4$. A quasiperiodic time dependence has been found at $R = 1.8 \cdot 10^4$, and aperiodic convection occurs at even higher Rayleigh numbers as shown in Fig. 10. The aperiodic type of convection appears to be even

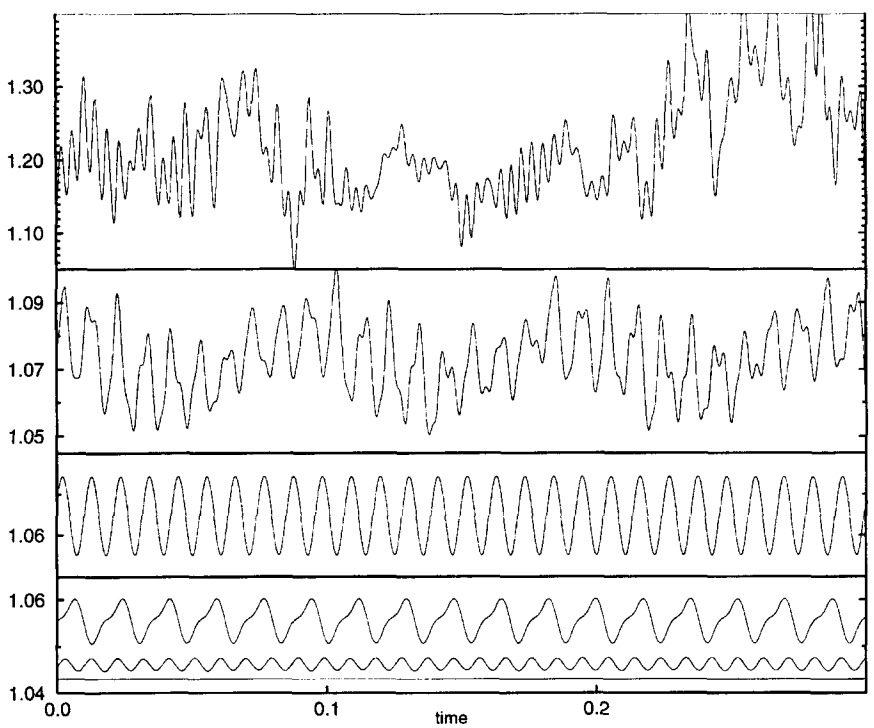

Fig. 10. The time dependence of the Nusselt number for time dependent convection in the cases corresponding to $R = 10 \times 10^3, 12 \times 10^3, 14 \times 10^3, 16 \times 10^3, 18 \times 10^3$ and 20×10^3 (from bottom to top).

better suited for a high average heat transport. The relative strong time dependence suggests that the constraint of rotation is partially removed and that hot parcels of fluid are impinging on the cold boundary and vice versa. Another cause for the increased convective heat transport is the fact that at Rayleigh numbers of the order $2 \cdot 10^4$ strong convection flows begin to appear in the polar regions, i.e. inside the cylindrical surface touching the equator of the inner sphere. Nevertheless the convection flow still remains symmetric with respect to the equatorial plane at $R = 2 \cdot 10^4$. A more detailed study of the various types of non-linear convection requires a survey of the parameter space. But such a study clearly goes beyond the scope of the present paper.

7. Concluding discussion

The results presented in this paper have been obtained primarily for the problem of the onset of convection. By covering a wider range of parameters than previous studies we have been able to demonstrate new features such as the multi-hump solutions which occur between the columnar modes and the equatorially attached convection modes. The equatorial approximation is especially suitable to describe the latter type of modes with a much reduced numerical effort. It is also readily applicable in the case of other boundary conditions since the shooting method permits a much simpler incorporation of boundary conditions than a Galerkin method. As an example we mention the case of rigid boundaries which will exhibit Ekman layers near the walls. At low and intermediate values of τ the critical Rayleigh number for onset of convection will differ from values found in the case of stress-free boundaries. But for high values of τ the difference diminishes as has been shown by Roberts (1965) except in the limit of low Prandtl number where different power laws for the dependence of R_c on τ persist (Zhang, 1995).

Only some typical examples for the evolution of non-linear convection have been considered. But it has become apparent that a variety of dynamical behavior must be expected in dependence on the parameters of the problem. There are many more types of oscillations in low Prandtl number fluids than in the high Prandtl number limit which has been previously investigated by Zhang (Zhang, 1991, Zhang, 1992). The most remarkable finding is the strong promotion of the heat transport by the onset of vacillations. It will be of interest to study in more detail the extent to which the time dependence can be understood in an approximate sense as the superposition of modes drifting at different rates. Such an integration was found in the special case $P = 1$ in the cylindrical annulus by Schnaubelt and Busse (1992) and by Sun et al. (1993) in the spherical case.

Acknowledgements

The research reported in this paper has been supported by the Deutsche Forschungsgemeinschaft under Grant Bu589/1. We are grateful to Dr. A. Tilgner for providing a program with which some of the time dependent computations have been done.

References

Busse, F.H., 1970a. Thermal instabilities in rapidly rotating systems. J. Fluid Mech., 44: 441–460.

Busse, F.H., 1970b. Differential rotation in stellar convection zones. Astrophys. J., 159: 629–639.

Busse, F.H., 1973. Differential rotation in stellar convection zones II. Astron. Astrophys., 28: 27–37.

Chandrasekhar, S., 1961. Hydrodynamic and Hydromagnetic Stability. Clarendon Press, Oxford.

Clever, R.M. and Busse, F.H., 1979. Nonlinear properties of convection rolls in a horizontal layer rotating about a vertical axis. J. Fluid Mech., 94: 609–627.

Geiger, G. and Busse, F.H., 1981. On the onset of thermal convection in slowly rotating fluid shells. Geophys. Astrophys. Fluid Dyn., 18: 147–156.

Press, W.H., Flannery, B.P., Teukolsky, S.A. and Vetterling, W.T., 1986. Numerical Recipes. Cambridge University Press.

Roberts, P.H., 1965. On the thermal instability of a highly rotating fluid sphere. Astrophys. J., 141: 240–150.

Roberts, P.H., 1968. On the thermal instability of a rotating fluid sphere containing heat sources. Phil. Trans. R. Soc. London A, 263: 93–117.

Schnaubelt, M. and Busse, F.H., 1992. Convection in a rotating cylindrical annulus, part 3: vacillating and spherical modulated flows. J. Fluid Mech., 245: 155–173.

Sun, Z.-P., Schubert, G. and Glatzmaier, G.A., 1993. Transitions to chaotic thermal convection in a rapidly rotating spherical fluid shell. Geophys. Astrophys. Fluid Dyn., 69: 95–131.

Veronis, G., 1968. Large-amplitude Bénard convection in a rotating fluid. J. Fluid Mech., 31: 113–139.

Zhang, K., 1991. Vacillating convection in a rotating spherical

fluid shell at infinite Prandtl number. J. Fluid Mech., 228: 607–628.

Zhang, K., 1992. Convection in a rapidly rotating spherical shell at infinite Prandtl number: transition to vacillating flows. Phys. Earth Planet. Inter., 72: 236–248.

Zhang, K., 1994. On coupling between the Poincaré equation and the heat equation. J. Fluid Mech., 268: 211–229.

Zhang, K., 1995. On coupling between the Poincaré equation and the heat equation: non-slip boundary condition. J. Fluid Mech., 284: 239–256.

Zhang, K.-K. and Busse, F.H., 1987. On the onset of convection in rotating spherical shells. Geophys. Astrophys. Fluid Dyn., 39: 119–147.